Molecular Catalysis 493 (2020) 111072

Contents lists available at ScienceDirect

Molecular Catalysis

journal homepage: www.elsevier.com/locate/mcat

$Cu^{I}BiOI$ is an efficient novel catalyst in Ullmann-type CN− couplings with wide scope—A rare non-photocatalyic application

Gábor Varga[a,b,*], Marianna Kocsis[a,b], Ákos Kukovecz[c], Zoltán Kónya[c,d], Igor Djerdj[e], Pál Sipos[b,f], István Pálinkó[a,b,*]

[a] Department of Organic Chemistry, University of Szeged, Dóm Tér 8, Szeged, H-6720 Hungary
[b] Materials and Solution Structure Research Group, and Interdisciplinary Excellence Centre, Institute of Chemistry, University of Szeged, Aradi Vértanúk tere 1, Szeged, H-6720, Hungary
[c] Department of Applied and Environmental Chemistry, University of Szeged, Rerrich Béla tér 1, Szeged, H-6720, Hungary
[d] MTA-SZTE Reaction Kinetics and Surface Chemistry Research Group, Rerrich Béla tér 1, Szeged, H-6720, Hungary
[e] Department of Chemistry, J. J. Strossmayer University of Osijek, Cara Hadrijana 8/a, Osijek, HR-31000, Croatia
[f] Department of Inorganic and Analytical Chemistry, University of Szeged, Dóm tér 7, Szeged, H-6720, Hungary

ARTICLE INFO

Keywords:
Synthesis of $Cu^{I}BiOI$
Structural characterization
Spectroscopies (far IR, Raman, UV-DR, XP, ICP-MS)
Electron microscopies (SEM, TEM)
Thermal methods
−Ullmann-type CN coupling reactions

ABSTRACT

Preparation of a new, mixed-cationic layered $Cu^{I}BiOI$ was prepared and its non-photocatalytic catalytic properties were explored. This solid substance had BiOI-like, lamellar and deflected structure resulting from Cu^{I} ion incorporation in the Bi_2O_2 layers. The as-prepared substance was fully characterized by XRD, Raman, far IR, UV−DR, XP spectroscopies, thermal (TG-DTG) and analytical (ICP-MS, SEM-EDX) methods, electron microscopies (SEM, TEM) as well as BET surface area measurements. By performing Ullmann-type CN− coupling reactions between aryl halides and aqueous ammonia, its catalytic capabilities were tested. The effects of solvents, added base and catalyst loading as well as reaction time and reaction temperature were scrutinized, and a green way for the reaction was identified. The recyclability of the catalyst without the loss of activity and its general applicability for a wide range of aryl halides were also demonstrated.

1. Introduction

Since the low-cost, easy availability and low-toxicity of bismuth and its compounds [1] qualify it as green element [2], bismuth compounds have been utilized as efficient low-cost environmentally benign Lewis acidic catalysts in a wide variety of synthetic organic transformations [3–5]. Many attempts were performed to design homogeneous bismuth catalysts for Strecker synthesis [6,7], Biginelli [8–12], Pictet–Spengler [13,14], aldol [15,16] and Michael reactions [17,18], Friedel-Crafts acylation [19–22], rearrangements (Fries, Beckmann, Ferrier) [23–26] as well as aromatization (Hantzsch) reactions [27]. However, few examples can only be found in the literature concerning the application of heterogeneous or heterogenized bismuth-containing systems in non-photocatalytic applications [28,29].

The main uses of bismuth-containing materials, the non-lamellar oxides [30], perovskites [31], lamellar double salts [32], oxohalides [33], perovskites [34] and superstructures [35,36] such as Sillen-Aurivillius [37] structures are in the field of photochemistry [38] or photovoltaic science [39].

For instance, bismuth oxohalides only gained attention, it was remarkable though, as photocatalysts [40]. Bismuth oxohalides with a tetragonal matlockite structure (space group P4/nmm) precipitated in lamellar structures consisting of [X–Bi–O–Bi–X] bonded layers are kept together with non-covalent interactions through the halogen···halogen close contacts along the c axis [41]. Generally, the photocatalytic capabilities of the BiOX systems could be enhanced by systematically varying the particle size of the materials [42], the surface-to-volume ratios [43], exchanging the counter ions [44] or modifying the porosity [45]. There are some studies, which concern doping of the parent BiOX materials with metal ions. Ca^{II} [46], Sr^{II} [47], Pb^{II} [48], Mn^{II} [49], Fe^{III} [50], Co^{II} [51] and Cu^{II} [52–54] were used for this purpose, and they usually enhanced the photocatalytic activities of the parent substance. For instance, Cu^{II} doping meant deposition of Cu^{II} salt onto the surface of BiOCl, and visible light photoactivity was observed [52].

In this contribution, the insertion of Cu^{I} ions, proven by a range of instrumental methods, is described into the structure of BiOI for the first time. The material obtained was tested as catalyst in a non-photocatalytic reaction, in an Ullmann-type reaction. It is the CN− coupling

* Corresponding authors at: Department of Organic Chemistry, University of Szeged, Dóm Tér 8, Szeged, H-6720 Hungary.
E-mail addresses: gabor.varga5@chem.u-szeged.hu (G. Varga), palinko@chem.u-szeged.hu (I. Pálinkó).

https://doi.org/10.1016/j.mcat.2020.111072
Received 24 April 2020; Received in revised form 28 May 2020; Accepted 6 June 2020

reaction catalyzed by copper species, known for a long time [55], but intensively researched and applied in recent times as well [56–60]. This method has now acquired great significance considering its potential in environmentally benign uses in drug-related syntheses [61]. It is to be noted that, by applying organic additives, numerous methods for copper-mediated reactions under homogeneous conditions have been developed [62]. On the contrary, the studies focusing at reusable catalysts only form a small fraction of the published articles. In these works, various types of supports were applied for anchoring copper species of different oxidation states to perform condensation of unsaturated N heterocycles with aryl halides [63–65]. Furthermore, the catalytic performance of self-supported catalysts were only described in one paper, the application of Cu_2O-coated Cu(0) or nano-Cu(0) provided with acceptable yield [66]. Until now, Cu(I) inserted USY (zeolite) seemed to be the most efficient heterogeneous Cu-containing system [67].

The results obtained and their interpretation are communicated in the followings.

2. Experimental

2.1. Materials, synthetic and pretreatment procedures

All the chemicals ($Bi(NO_3)_3 \times 5\ H_2O$, CuI, cc. HNO_3, KI, aryl halides (iodobenzene; chlorobenzene; bromobenzene; 2-chlorophenol; 3-chlorophenol; 1-chloronaphtalene, 1,2-dichlorobenzene; 1,3-dicglorobenzene; 1-chloro-2-nitrobenzene; 1-chloro-3-ntirobenzene; 2-chloropyridine; 4-chloroquinoline and 10-chloro-9-anthraldehyde), 25 % NH_3 aqueous solution, applied bases (K_2CO_3, K_3PO_4, Cs_2CO_3, pyridine, piperidine), OH–L-proline, Na_2SO_4, hexane, ethyl acetate, diethyl ether, applied solvents (dimethyl sulfoxide (DMSO), acetone, toluene, tetrahydrofuran (THF), 96 % ethanol) were purchased from Sigma-Aldrich in analytical purity and were used as received. Purified water was produced by reverse osmosis and UV irradiation processes by a Puranity TU 3 + UV/UF system (VWR).

The catalysts were prepared by a modified co-precipitation method. Aqueous solution of KI (V = 25 mL; c = 0.12 M) and varying amounts of CuI (n = 5.25×10^{-4} – 2.1×10^{-3} mol) were made and treated by 15-minute-long ultrasonic irradiation. In another flask, $Bi(NO_3)_3 \times 5\ H_2O$ (n = 1.2×10^{-3} mol) was dissolved in 25 ml of 5 % HNO_3. This solution was prepared with 60-minute-long ultrasonic irradiation. Then, under continuous stirring, the Bi^{III}-containing solution was added dropwise to the Cu^{I}-containing solution. The mixture was stirred at room temperature for 60 min, then at 90 °C for 168 h. The materials obtained were separated by centrifugation (1800 rpm) followed by filtration, washed with hot (~60 °C) distilled water and ethanol several times, and dried at 60 °C for 24 h. BiOI, for comparison, was made in the same way, but without CuI.

$Cu_{0.48}Bi_{2.52}O_4$ was obtained by heat treatment of the Cu^{I}BiOI material at 550 °C for 2 h. α-Bi_2O_3 was produced by heat treatment of BiOI catalyst at 750 °C for 2 h.

2.2. Methods of structural characterization

X-ray diffraction (XRD) patterns were recorded on a Rigaku XRD-MiniFlex II instrument applying Cu Kα radiation (λ = 0.15418 nm) with 40 kV accelerating voltage at 30 mA.

The morphology of the freshly prepared samples was studied by scanning electron microscopy (SEM). The SEM images were registered on an S-4700 scanning electron microscope (SEM, Hitachi, Japan) with accelerating voltage of 10–18 kV. EDX data were obtained with a Röntec QX2 energy dispersive microanalytical system from two different parts of the sample. The coupled system also provided with the elemental map. More detailed images of the as-prepared samples were produced by transmission electron microscopy (TEM). For these measurements, a FEI Tecnai™ G2 20 X-Twin type instrument was used operating at an acceleration voltage of 200 kV.

The Raman spectra were recorded with a Thermo Scientific TM DXRTM Raman microscope at an excitation wavelength of 635 nm applying 10 mW laser power and averaging 20 spectra with an exposition time of 6 s. UV–DR spectra were registered on an Ocean Optics USB4000 spectrometer with a DH-2000-BAL UV–Vis–NIR light source measuring diffuse reflectance using $BaSO_4$ as reference. The spectra were analyzed with the SpectraSuite package. For the identification of MO−/I vibrations, the far IR spectra were recorded with a BIO-RAD Digilab Division FTS-40 vacuum FT–IR spectrophotometer (4 cm^{-1} resolution, 256 scans). The Nujol mull technique was used between two polyethylene windows (the suspension of 10 mg sample and a drop of Nujol mull).

X-ray photoelectron spectra (XPS) were recorded using a SPECS instrument equipped with a PHOIBOS 150 MCD 9 hemispherical electron energy analyzer using Al Kα radiation ($h\nu$ = 1486.6 eV). The X-ray gun was operated at 210 W (14 kV, 15 mA). The analyzer was operated in the FAT mode, with the pass energy set to 20 eV. The step size was 25 meV, and the collection time in one channel was 250 ms. Typically, 5–10 scans were added to acquire a single spectrum. Energy referencing was not applied. In all cases the powder-like samples were evenly laid out on one side of a double-sided adhesive tape, the other side being attached to the sample holder of the XPS instrument. The samples were evacuated at room temperature, and then inserted into the analysis chamber of the XPS instrument.

BET surface area measurements were performed on a NOVA3000 (Quantachrome) instrument. The samples were degassed with N_2 at 100 °C for 5 h under vacuum to clean the surface of adsorbed materials. The measurements were performed at the temperature of liquid N_2.

The thermal behavior of the samples were investigated by thermogravimetry (TG) and differential thermogravimetry (DTG). The samples were studied in a Setaram Labsys derivatograph operating in air at 5 °C min^{-1} heating rate. For the measurements, 20–30 mg of the samples were applied.

The actual ratios of metal ions in the oxohalides were determined by Agilent 7700× Inductively Coupled Plasma Mass Spectrometer (ICP–MS). Multielemental internal standard was used for each measurement. Before measurements, few milligrams of the samples measured by analytical accuracy were dissolved in 5 ml of cc. HNO_3. After dissolution, the samples were diluted with distilled water to 100 ml and filtered.

2.3. Catalytic procedure for the Ullmann-type CN− coupling reactions

For testing the catalytic capabilities of oxohalides, Ullmann-type CN− coupling reactions were carried out. The mixtures of CuI (0.01–0.1 mmol) or Cu^{I}BiOI (0.01–0.1 mmol for Cu) or BiOI (0.01–0.1 mmol for Bi) catalyst, organic additive (0.05 mmol, OH–L-proline only for CuI), (hetero)aryl halide (0.5 mmol), base (1.0 mmol) and aqueous ammonia (1.0 mmol) as well as 3.0 ml of solvent were stirred in a 10 ml flask in N_2 atmosphere for 1–24 h, at 25–110 °C. After cooling to room temperature, the crude product was diluted with ethyl acetate (~40 ml). The organic phase was separated and the aqueous phase was extracted with ethyl acetate twice. The combined organic phase was dried over Na_2SO_4. The product was purified by silica gel chromatography using solvent mixtures (ethyl acetate/hexanes, diethyl ether/hexanes).

At the end of the reactions, the mixtures were analyzed on a Hewlett-Packard 5890 Series II gas chromatograph equipped with flame ionization detector using an Agilent HP-1 column and the internal standard technique using toluene. The temperature was increased in stages from 50 °C to 300 °C. The products were identified *via* using authentic samples.

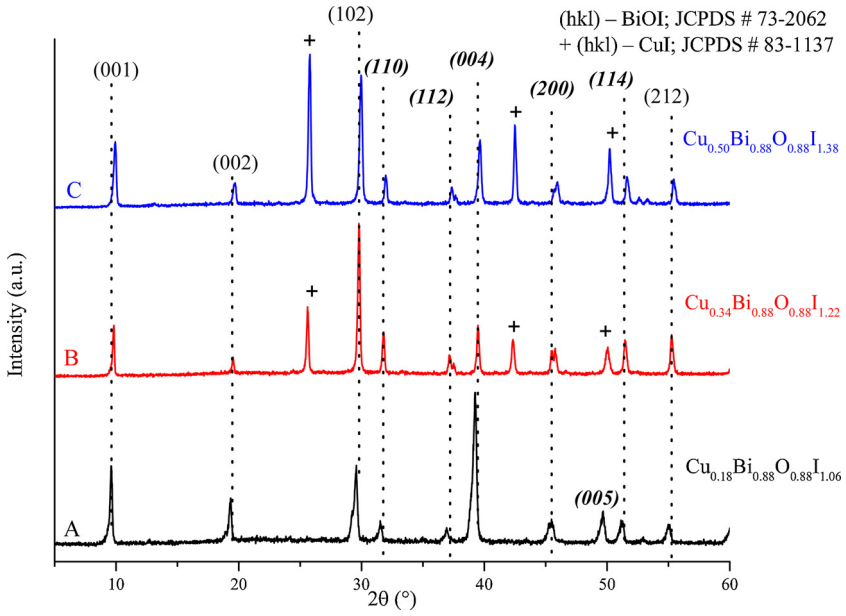

Fig. 1. XRD patterns of Cu@BiOI heterostructures with various amounts of added CuI. A: 5.25 × 10^{-4} mol CuI; B: 1.05 × 10^{-3} mol CuI; C: 2.10 × 10^{-3} mol CuI.

3. Results and discussion

3.1. Structural analysis of the $Cu^{I}BiOI$ material

Fig. 1 displays the XRD patterns of $Cu^{I}BiOI$ prepared by modified co-precipitation with various amounts of CuI. The diffractograms confirm the formation of well-crystallized solid samples with tetragonal unit cell of *P4/nmm* space group, an analogous structure to layered bismuth oxoiodide (JCPDS File No. 73-2062) [68]. However, the intensities of several peaks changed significantly (the Miller indices of the relevant peaks are written in bold) indicating possible Cu^{I} insertion. It is to be noted that the ratio of CuI (JCPDS # 83-1137) side-product increased with increasing Cu^{I} dosage. Phase purity was achieved by using 1:6 nominal molar ratio of Cu^{I} and Bi^{III} cations (Fig. 1, trace A). On the basis of ICP-MS and SEM-EDX measurements, the actual composition was found to be $Cu_{0.18}Bi_{0.88}O_{0.88}I_{1.06}$ for the phase-pure product. On performing a 550 °C heat treatment on the phase-pure product, a spinel structure, analogous to $Cu^{I}Bi_2O_4$, could be produced (Fig. S1, trace B – "S" is used as prefix for the figures and the table in the Supplementary Information file).

The lattice constants for the $Cu^{I}BiOI$ product (a = b = 3.989 Å; c = 9.416 Å) are very similar to those of the non-modified BiOI [69]. It may be assumed that Cu^{I} ions replaced some of the Bi^{III} ions in the layers largely keeping original BiOI structure, but making it somewhat deflected, since the Cu^{I} ion is smaller than the Bi(III) ion. Similar phenomenon was observed when Cu^{I} ion was inserted into CeO_2, which also had tetragonal structure [70].

In order to collect further proofs for the insertion of Cu^{I} ions into the $[Bi_2O_2]$ units, the far IR and the Raman spectra were recorded. The far IR spectrum of the phase-pure $Cu^{I}BiOI$ sample is shown in Fig. 2, trace A. This spectrum exhibits two characteristics bands at 450 and 618 cm^{-1}. The strong absorption band observed at 450 cm^{-1} is related to the stretching mode of the BiO− bonds of the BiO_6 octahedron (ν(BiO−)) [71]. It is shifted to the lower energy compared to the previous published wavenumber value of pure BiOI (489 cm^{-1}). This shift of the halogen insensitive band is attributed to the structural distortion of $[Bi_2O_2]$ units, in agreement with the experiences collected for modified Sillén structures [72]. Comparing to other copper oxides, the small peak at 648 cm^{-1} is identified as the shifted stretching vibration of the Cu–O band in the assumed tetrahedral cell [73]. This shift can also be assigned to the insertion of the Cu^{I} ion into the lamellar structure.

The Raman spectrum of material produced is seen in Fig. 2, trace B. It displays four Raman bands at 87, 112, 148 and 358 cm^{-1}. The bands at 87 and 148 cm^{-1} are associated with the A_{1g} mode of the (Bi–X) stretching vibrations of the iodine centers around the tetragonal $[001]_h$ direction [74] and E_g mode of the pure Bi(–X) vibration in the tetragonal $[001]_h$ plane. These are halogen-sensitive bands [75]. These peaks are centered at exactly the same position as for BiOI indicating that the Bi–X units are the same [76]. The two bands at around 112 and 358 cm^{-1} are the shifted A_{1g} mode of translational vibration of the CuO_4 plane along the Z-axis [77] and the shifted B_g mode related to the oxygen atom vibrations in the Cu–O–M lattice [78]. These observations verify that all of the Raman and IR vibrations bands related to Bi–O or Cu–O units are shifted confirming again that Cu^{I} insertion occurred, indeed.

To investigate the oxidation states of the cationic components of the $Cu^{I}BiOI$ material, X-ray photoelectron spectroscopy analysis was carried out, and the results are displayed in Fig. 2/C and D. Fig. 2/C presents the 4f region of bismuth, which includes two well-resolved peaks at around 159.65 and 165.90 eV. The binding energies correspond to Bi $4f_{7/2}$ and Bi $4f_{5/2}$, respectively, demonstrating that the main oxidation state of Bi in the samples was +3 [79]. Fig. 2/D shows the core level of the Cu 2p spectra. The location of the deconvoluted main peak related to the Cu $2p_{3/2}$ transition indicates the presence of Cu° or Cu^{I} species in the structure [80]. The absence of the shake-up lines (satellite peaks) attest that the main peak can be attributed to Cu^{I} valance state [81]. Cu 2p peak overlaps with two iodine peaks; the 930.20 eV binding energy is identified as I $3p_{1/2}$ transition [82]. The other, broadened peak at about 926.10 eV due to Jahn-Teller effect, caused distortion in the layered structure resulting in lower binding energies (926.10 eV) for neighboring iodines [83]. The 3p transitions of iodine are very sensitive to distortions contrary to the 3d peaks. The peak located at ~620 eV (Fig. S2) belongs to the 3d transition of iodine species confirming its presence in chemical bond [84]. The peak at ~533 eV is the oxygen [85]. All these results indicate the formation of a deflected lamellar $Cu^{I}BiOI$ structure as well.

In order to further verify Cu^{I} insertion, the optical behaviour of BiOI and $Cu^{I}BiOI$ were compared (Fig. 3/A and B). The diffuse reflectance spectra (Fig. 3/A) of the BiOI and the $Cu^{I}BiOI$ samples have similar absorption profiles and maxima; however, due to Cu^{I} insertion [86], all characteristic transitions underwent red shift. Since new bands did not appear, thus, no new material was formed, this is an indication of Cu^{I}

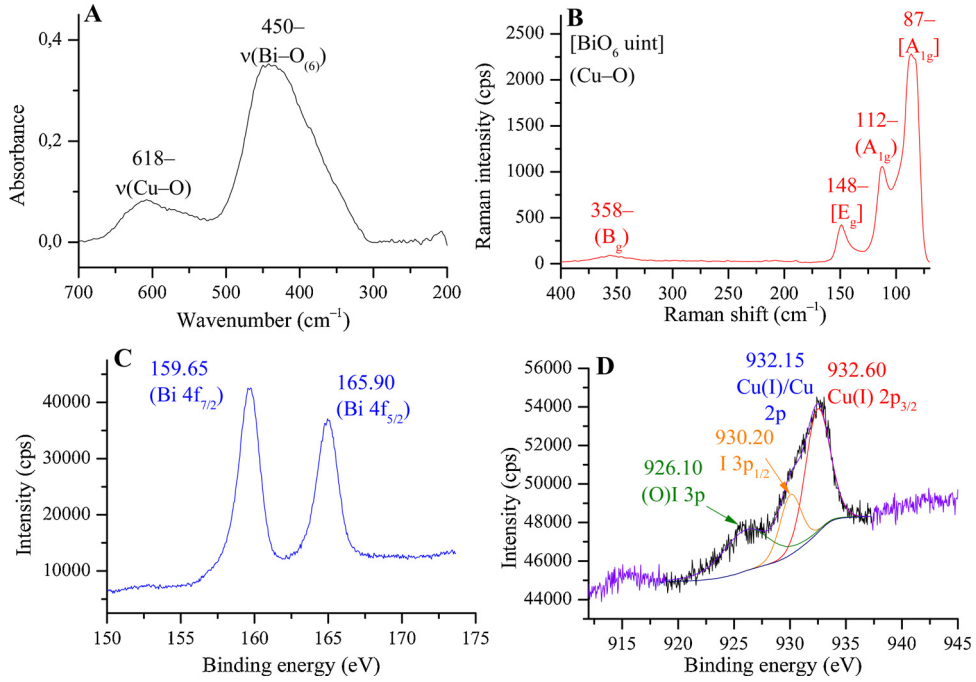

Fig. 2. A: far IR, B: Raman, C: Bi 4f XP and D: deconvoluted Cu 2p XP spectra of the as-synthesized phase-pure Cu-containing BiOI analogue.

insertion into the BiOI structure. The calculated band gaps (Fig. 3/B) also differ indicating structural modification.

TG-DTA measurements were also carried out to investigate the thermal behaviour of pure and Cu-modified BiOI. Three endothermic peaks, centered at 215, 486 and 695 °C, appeared during the calcination process of BiOI (Fig. 3/C). In the TG-DTA curve, the first peak (centered at 215 °C) corresponds to BiOI to $Bi_4O_5I_2$ transformation [87]. The second main peak (centered at 486 °C) can be associated with the transformation of $Bi_4O_5I_2$ to Bi_5O_7I [88]. The third peak is related to total calcination to form α-Bi_2O_3, which is identified by X-ray diffractometry (Fig. S1, trace E – JCPDS # 41-1449) [89].

Three main peaks appeared during calcination of Cu^{I}BiOI as well (Fig. 3/D). The first weight loss around 160 °C may be attributed to the phase transformation of Cu^{I}BiOI into a lower symmetry iodine-containg phase. The second endothermic peak centered at about 299 °C may be assigned to the collapse of the lamellar framework resulting in a mixed CuBiO(I) structure [90]. The weight loss observed around 488 °C indicates the formation of $Cu_{0.48}Bi_{2.42}O_4$ spinel oxide, identified by X-ray diffractometry (Fig. S1, trace B).

The as-prepared Cu^{I}BiOI particles are non-uniform in shape, and consist of numerous nanoparticles as the TEM images attest (Fig. 4/A–C). Small-sized nanoballs (C) build up the nanostructures with

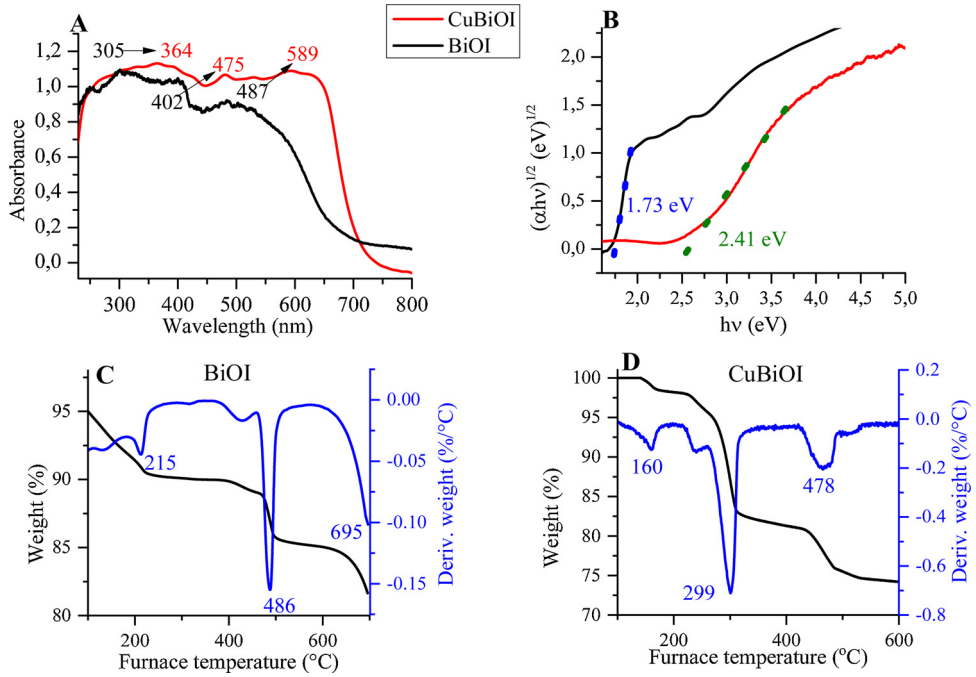

Fig. 3. A: UV–DR spectra, B: $(\alpha h\upsilon)^{1/2}$ vs. energy ($h\upsilon$) plot for calculating the band gap energy and TG/DTG (C and D) curves for the as-prepared phase-pure C: BiOI and D: the Cu^{I}BiOI.

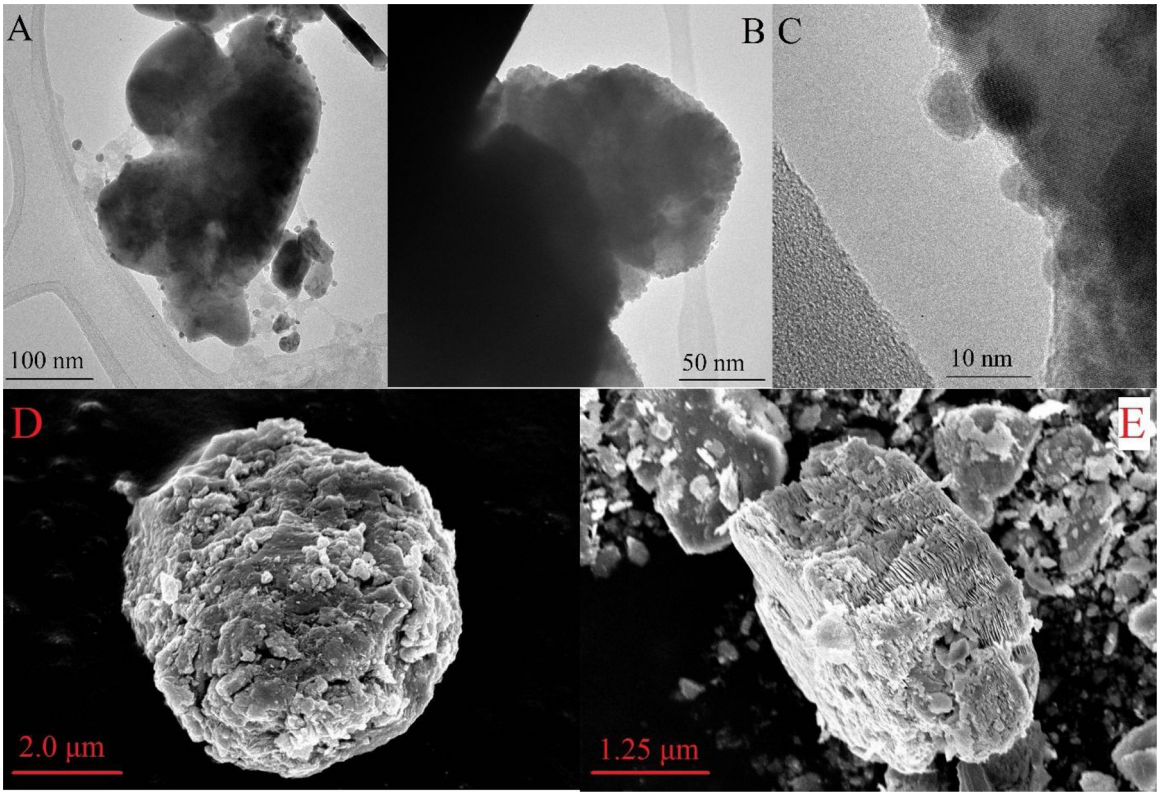

Fig. 4. A–C: TEM images and D–E: SEM images of the $Cu^{I}BiOI$ material.

thicknesses of 80–150 nm and lengths of approximately 200–800 nm. SEM images (Fig. 4/D–E) reveal non-porous lamellar structure with cauliflower morphology. The non-porous structure was confirmed by BET measurement (Fig. S3) as well. The isotherm is of type IV isotherms with H_3 hysteresis loop, which describes lamellar structure without hierarchically ordered pores [91]. Low specific surface areas (45–65 m^2/g) were obtained for both the freshly prepared BiOI and $Cu^{I}BiOI$.

3.2. Catalytic behavior of $Cu^{I}BiOI$

Copper-catalyzed coupling reaction of ammonia with aryl halides have attracted much attention for a long time [56]. The organic additive promoted Ullmann reactions gave major "push" to this field [57]. One of the most attractive homogeneous systems consists of CuI and various organic promoters [58].

Our as-prepared $Cu^{I}BiOI$ material and for comparison the BiOI substance were tested in this reaction (Scheme 1) in the presence or without organic additive and the homogeneous variant using CuI was also probed (Fig. 5).

To much of our surprise the reaction proceeded over BiOI using Bi^{III} ions as active centers. As it is expected the Cu^{I}-containing catalysts (either homogeneous or heterogeneous) were significantly more active. It is to be noted that over the heterogeneous catalyst there was no need for organic additive, i.e. the reaction was greener than the one promoted by the homogeneous catalyst. It is also important to point out that as far as activity is concerned, $Cu^{I}BiOI$ was competitive with the homogeneous CuI − HO-L-proline containing system, in which HO–L-proline was found to be the best performing organic additive [92]. It is to be noted that the selectivity over both as-prepared composites and with the homogeneous catalysts were 100 % for the amine product.

We hoped to further improve the performance of $Cu^{I}BiOI$ by optimizing the reaction conditions. Therefore, the effects of all relevant parameters were explored, such as catalyst loading (Fig. S5; optimum: 4 %), type of base (Table S1; optimum: K_3PO_4), solvents and reaction temperatures (Fig. S6) A moderately high temperature, 80 °C, at which the original structure of $Cu^{I}BiOI$ remained intact, and a green solvent mixture, H_2O/ethanol (Figs. S5, S6) were found to be optimal. $Cu^{I}BiOI$ catalyst is assumed to provide the most effective catalytic behavior from the presented systems, because not only the Cu(I) centers but also Bi(III) Lewis acidic centers take part in the catalytic process. Accordingly, in this case, a bifunctional heterogeneous system is operational. A possible reaction mechanism has been outlined in the Supplementary Information document (Scheme S1).

The recyclability of $Cu^{I}BiOI$ catalyst was checked in six consecutive runs under the optimal reaction conditions (Fig. 6). Slight deactivation was only observed. Leaching did not occur by ICP-MS measurements, and the lamellar structure was retained with some loss of crystallinity as confirmed by X-ray diffractometry (Fig. S1, trace C). In order to ensure the catalyst is indeed stable, the recycling measurements were repeated with lower amount catalyst (0.02 mmol) removing the

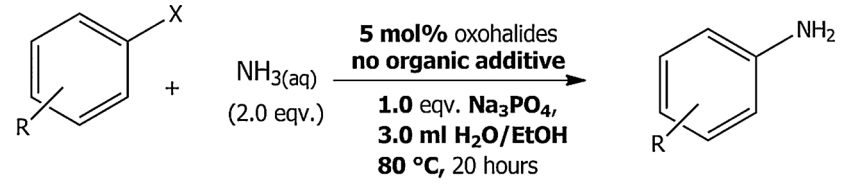

X = I, Br, Cl; R = Cl, OH, Ar, NO_2

Scheme 1. Ullmann-type CN− coupling reaction between aryl halides and aqueous ammonia catalyzed by oxohalides.

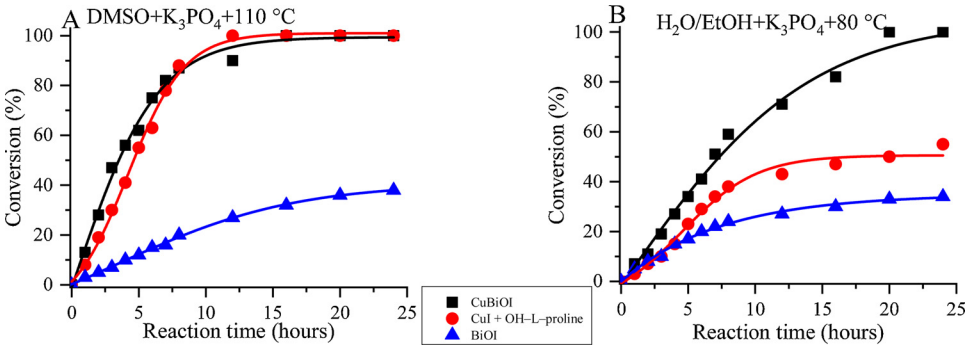

Fig. 5. Ullmann-type CN– coupling reaction between chlorobenzene and aqueous ammonia. Reaction conditions: 1.0 mmol of aqueous ammonia; 0.5 mmol of chlorobenzene; 0.04 mmol (0.06 mmol in the homogeneous case) of catalyst; 0.5 mmol of base; 3.0 ml of solvent; 0.05 mmol of organic additive (hydroxy–L-proline, if it is necessary).

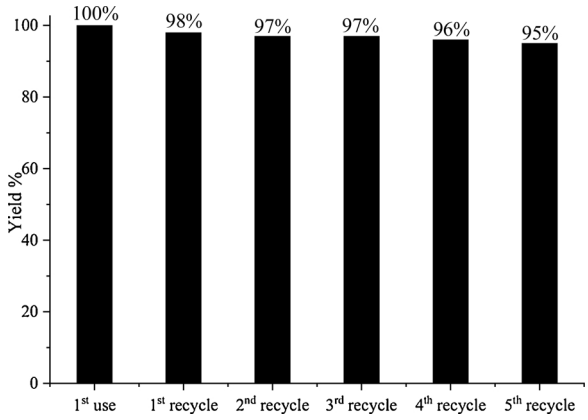

Fig. 6. Recyclability of the as-prepared $Cu^{I}BiOI$ material tested in Ullmann-type CN– coupling reaction between chlorobenzene and aqueous ammonia. The optimized conditions: 1.0 mmol aqueous ammonia; 0.5 mmol chlorobenzene; 0.04 mmol catalysts; 0.5 mmol K_3PO_4; 3 ml EtOH/water (1:1; v/v%); T = 80 °C; t = 20 h.

conversion from the vicinity of 100 % (Fig. S7) [93]. Fortunately, the obtained results were in line with previously concluded statement.

The reaction was extended to various aromatic halides using mostly the above-described optimum conditions (Table 1). The N-containing heterocycles and anthracene derivative only required lengthening the reaction time. The newly synthesized $Cu^{I}BiOI$ catalyst proved to be efficient with all the probe molecules. Interestingly, the presence of electron-withdrawing groups was found to be more advantageous than that of the electron-donating ones.

Table 1
Scope of $Cu^{I}BiOI$ catalyzed coupling reaction of aryl halides and aqueous ammonia[a].

Reactant	Yield (%)
	100
	100
	100
	76
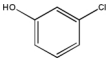	79
	85
	100
	98
	99
	98
	75*
	71*
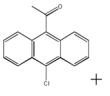	87*

[a] Reactions conditions: 1.0 mmol of aqueous ammonia; 0.5 mmol of aryl halide; 0.04 mmol of catalyst; 0.5 mmol of K_3PO_4; 3 ml of EtOH/water (1:1; v/v%); T = 80 °C; t = 20 h.
* Reaction time: 40 h; +: determined by NMR.

4. Conclusions

In this study, a novel mixed-cationic material of $Cu_{0.18}Bi_{0.88}O_{0.88}I_{1.06}$ composition with somewhat distorted layered structure with Cu^{I} ions in the layers was prepared, characterized and used as efficient and selective catalyst for the Ullmann-type CN– coupling reaction using green reaction conditions: H_2O/ethanol solvent mixture, no organic additive, mild reaction temperature and heterogeneous catalyst with excellent recycling ability.

Also, as an unexpected "side result", the catalytic activity of Bi^{III} cations in Ullmann-type reaction was demonstrated for the first time.

Authors statement

All the authors contributed significantly to the manuscript.

G. Varga and M. Kocsis were involved in the catalyst synthesis and catalytic testing part.

G. Varga wrote the first draft of the manuscript.

A. Kukovecz, Z. Kónya, Igor Djerdj and P. Sipos were involved in the instrumental characterization part and in putting together the relevant part of the manuscript.

I. Pálinkó conceptualized and supervised the project, wrote the final version of the manuscript and did the revision.

Declaration of Competing Interest

The authors declare no conflict of interests.

Acknowledgements

This work was supported by the Hungarian Government and the European Union through grant GINOP-2.3.2-15-2016-00013. The financial helps is highly appreciated. One of us, G. Varga thanks for the postdoctoral fellowship under the grant PD 128189.

Appendix A. Supplementary data

Supplementary material related to this article can be found, in the online version, at doi:https://doi.org/10.1016/j.mcat.2020.111072.

References

[1] S. Repichet, A. Zwick, L. Vendier, C. Le Roux, J. Dubac, A practical, cheap and environmentally friendly preparation of bismuth (III) trifluoromethanesulfonate, Tetrahedron Lett. 43 (2002) 993–995.
[2] N. Irwing-Sax, R.J. Bewis, Dangerous Properties of Industrial Materials, Van Nostram Reinhold, New York, 1989, pp. 283–284.
[3] R. Mohan, N. Leonard, L. Wieland, Applications of bismuth (III) compounds in organic synthesis, Tetrahedron 58 (2002) 8373–8397.
[4] H. Qin, N. Yamagiwa, S. Matsunaga, M. Shibasaki, H. Qin, N. Yamagiwa, S. Matsunaga, M. Shibasaki, Bismuth-catalyzed intermolecular hydroamination of 1,3-dienes with carbamates, sulfonamides, and carboxamides, J. Am. Chem. Soc. 128 (2006) 1611–1614.
[5] X.C. Wang, R.L. Yan, M.J. Zhong, Y.M. Liang, X.C. Wang, R.L. Yan, M.J. Zhong, Y.M. Liang, Bi (III)-catalyzed intermolecular reactions of (Z)-pent-2-en-4-yl acetates with ethynylarenes for the construction of multisubstituted fluorene skeletons through a cascade electrophilic addition/cycloisomerization sequence, J. Org. Chem. 77 (2012) 2064–2068.
[6] S.K. De, R.A. Gibbs, Bismuth trichloride catalyzed synthesis of α-aminonitriles, Tetrahedron Lett. 45 (2004) 7407–7408.
[7] S. Solyntjes, B. Neumann, H.G. Stammler, N. Ignatev, B. Hoge, Bismuth perfluoroalkylphosphinates: new catalysts for application in organic syntheses, Chem. Eur. J. 23 (2017) 1568–1575.
[8] R. Varala, M.M. Alam, R.S. Adapa, R. Varala, M.M. Alam, S.R. Adapa, Bismuth triflate catalyzed one-pot synthesis of 3, 4-dihydropyrimidin-2 (1H)-ones: an improved protocol for the Biginelli reaction, Synlett (2003) 67–70.
[9] B.K. Banik, A.T. Reddy, A. Datta, C. Mukhopadhyay, Microwave-induced bismuth nitrate-catalyzed synthesis of dihydropyrimidones via Biginelli condensation under solventless conditions, Tetrahedron Lett. 48 (2007) 7392–7394.
[10] Y.T. Reddy, B. Rajitha, P.N. Reddy, B.S. Kumar, V.P. Rao, Y. Thirupathi Reddy, B. Rajitha, P. Narsimha Reddy, B. Sunil Kumar, V.P. Rao, Bismuth subnitrate catalyzed efficient synthesis of 3, 4-dihydropyrimidin-2(1H)-ones: an improved protocol for the Biginelli reaction, Synth. Commun. 34 (2004) 3821–3825.
[11] K. Ramalinga, P. Vijayalakshmi, T.N.B. Kaimal, Bismuth (III)-catalyzed synthesis of dihydropyrimidinones: improved protocol conditions for the Biginelli reaction, Synlett (2001) 863–865.
[12] S. Khademinia, M. Behzad, H.S. Jahromi, Solid state synthesis, characterization, optical properties and cooperative catalytic performance of bismuth vanadate nanocatalyst for Biginelli reactions, RSC Adv. 5 (2015) 24313–24318.
[13] C. Lherbet, D. Soupaya, C. Baudoin-Dehoux, C. Andre, C. Blonski, P. Hoffman, Bismuth triflate-catalyzed oxa-and thia-Pictet–Spengler reactions: access to iso-and isothio-chroman compounds, Tetrahedron Lett. 49 (2008) 5449–5451.
[14] B. Banerjee, Bismuth (III) triflate: an efficient catalyst for the synthesis of diverse biologically relevant heterocycles, ChemistrySelect 2 (2017) 6744–6757.
[15] J.M. Bothwell, S.W. Krabbe, R.S. Mohan, Applications of bismuth (III) compounds in organic synthesis, Chem. Soc. Rev. 40 (2011) 4649–4707.
[16] J. Jiang, Y. Meng, L. Zhang, M. Liu, Self-assembled single-walled metal-helical nanotube (M-HN): creation of efficient supramolecular catalysts for asymmetric reaction, J. Am. Chem. Soc. 138 (2016) 15629–15635.
[17] T. Ollevier, New trends in bismuth-catalyzed synthetic transformations, Org. Biomol. Chem. 11 (2013) 2740–2755.
[18] K.X. Xie, Z.P. Zhang, X. Li, Bismuth triflate-catalyzed vinylogous nucleophilic 1, 6-conjugate addition of para-quinone methides with 3-propenyl-2-silyloxyindoles, Org. Lett. 19 (2017) 6708–6711.
[19] K. Itami, Y. Ohashi, J. Yoshida, Triarylethene-based extended π-systems: programmable synthesis and photophysical properties, J. Org. Chem. 70 (2005) 2778–2792.
[20] E. Angelini, C. Balsamini, F. Bartoccini, S. Lucarini, G. Piersanti, Switchable reactivity of acylated α, β-dehydroamino ester in the Friedel − Crafts alkylation of indoles by changing the Lewis acid, J. Org. Chem. 73 (2008) 5654–5657.
[21] S. Gmouh, H. Yang, M. Vaultier, Activation of bismuth (III) derivatives in ionic liquids: novel and recyclable catalytic systems for Friedel − Crafts acylation of aromatic compounds, Org. Lett. 5 (2003) 2219–2222.
[22] Y. Gu, W. Huang, S. Chen, X. Wang, Bismuth (III) Triflate Catalyzed Three-Component reactions of indoles, ketones, and α-bromoacetaldehyde acetals enable indole-to-carbazole transformation, Org. Lett. 20 (2013) 4285–4289.
[23] O. Mouhtady, H. Gaspard-Iloughmane, N. Roques, C. Le Roux, Metal triflates–methanesulfonic acid as new catalytic systems: application to the Fries rearrangement, Tetrahedron Lett. 44 (2003) 6379–6382.
[24] K. Meraz, K.K. Gnanasekaran, R. Thing, R.A. Bunce, Bismuth (III) triflate catalyzed tandem esterification–Fries–oxa-Michael route to 4-chromanones, Tetrahedron Lett. 57 (2016) 5057–5061.
[25] Y. Torisawa, T. Nishi, J.I. Minamikawa, Interesting reaction of the indanone oximes under Beckmann rearrangement conditions, Bioorg. Med. Chem. Lett. 12 (2002) 387–390.
[26] J. Babu, A. Khare, Y. Vankar, $Bi(OTf)_3$ and SiO_2-$Bi(OTf)_3$ as effective catalysts for the Ferrier rearrangement, Molecules 10 (2005) 884–892.
[27] E. Rajanarendar, P. Ramesh, M. Srinivas, K. Ramu, G. Mohan, Solid-supported synthesis of isoxazole-substituted 1,4-dihydropyridines by modified Hantzsch method and their aromatization, Synth. Commun. 36 (2006) 665–671.
[28] P. Sreekanth, J.K. Park, J.W. Kim, T. Hyeon, B.M. Kim, Bismuth sulfonate immobilized on silica gel for allylation of aldehydes and synthesis of homoallylic amines, Catal. Lett. 96 (2004) 201–204.
[29] V.M. Alexander, A.C. Khandekar, S.D. Samant, Solvent-free iodination of arenes at room temperature, Synlett (2003) 1895–1897.
[30] D.P. Dutta, M. Roy, A.K. Tyagi, Dual function of rare earth doped nano Bi_2O_3: white light emission and photocatalytic properties, Dalton Trans. 41 (2012) 10238–10248.
[31] K. Sutthiumporn, T. Maneerung, Y. Kathiraser, S. Kawi, CO_2 dry-reforming of methane over $La_{0.8}Sr_{0.2}Ni_{0.8}M_{0.2}O_3$ perovskite (M = Bi, Co, Cr, Cu, Fe): roles of lattice oxygen on C–H activation and carbon suppression, Int. J. Hydrogen Energy 37 (2012) 11195–11207.
[32] H. Huang, Y. He, X. Li, M. Li, C. Zeng, F. Dong, X. Du, T. Zhang, Y. Zhang, $Bi_2O_2(OH)(NO_3)$ as a desirable $[Bi_2O_2]^{2+}$ layered photocatalyst: strong intrinsic polarity, rational band structure and {001} active facets co-beneficial for robust photooxidation capability, J. Mater. Chem. A 3 (2015) 24547–24556.
[33] J. Li, Y. Yu, L. Zhang, Bismuth oxyhalide nanomaterials: layered structures meet photocatalysis, Nanoscale 6 (2014) 8473–8488.
[34] K.M. McCall, C.C. Stoumpos, S.S. Kostina, M.G. Kanatzidis, B.W. Wessels, Strong electron–phonon coupling and self-trapped excitons in the defect halide perovskites $A_3M_2I_9$ (A = Cs, Rb; M = Bi, Sb), Chem. Mater. 29 (2017) 4129–4145.
[35] H. Fujito, H. Kunioku, D. Kato, H. Suzuki, M. Higashi, H. Kageyama, R. Abe, Layered perovskite oxychloride Bi_4NbO_8Cl: a stable visible light responsive photocatalyst for water splitting, J. Am. Chem. Soc. 138 (2016) 2082–2085.
[36] Z. Dai, F. Qin, H. Zhao, J. Ding, Y. Liu, R. Chen, Crystal defect engineering of aurivillius Bi_2MoO_6 by Ce doping for increased reactive species production in photocatalysis, ACS Catal. 6 (2016) 3180–3192.
[37] J. Fan, X. Hu, Z. Xie, K. Zhang, J. Wang, Photocatalytic degradation of azo dye by novel Bi-based photocatalyst Bi4TaO8I under visible-light irradiation, Chem. Eng. J. 179 (2012) 44–51.
[38] X. Lin, T. Huang, F. Huang, W. Wang, J. Shi, Photocatalytic activity of a Bi-based oxychloride Bi_3O_4Cl, J. Phys. Chem. B 110 (2006) 24629–24634.
[39] T. Singh, A. Kulkarni, M. Ikegami, T. Miyasaka, Effect of electron transporting layer on bismuth-based lead-free perovskite $(CH_3NH_3)_3Bi_2I_9$ for photovoltaic applications, ACS Appl. Mater. Interfaces 8 (2016) 14542–14547.
[40] K.L. Zhang, C.M. Liu, F.Q. Huang, C. Zheng, W.D. Wang, Study of the electronic structure and photocatalytic activity of the BiOCl photocatalyst, Appl. Catal. B 68 (2006) 125–129.
[41] M. Guan, C. Xiao, J. Zhang, S. Fan, R. An, Q. Cheng, J. Xie, M. Zhou, B. Ye, Y. Xie, Vacancy associates promoting solar-driven photocatalytic activity of ultrathin bismuth oxychloride nanosheets, J. Am. Chem. Soc. 135 (2013) 10411–10417.
[42] Q. Zhang, E. Uchaker, S.L. Candelaria, G. Cao, Nanomaterials for energy conversion and storage, Chem. Soc. Rev. 42 (2013) 3127–3171.
[43] X. Chen, C. Li, M. Grätzel, R. Kostecki, S.S. Mao, Nanomaterials for renewable energy production and storage, Chem. Soc. Rev. 41 (2012) 7909–7937.
[44] J. Henle, P. Simon, A. Frenzel, S. Scholz, S. Kaskel, Nanosized BiOX (X = Cl, Br, I) particles synthesized in reverse microemulsions, Chem. Mater. 19 (2007) 366–373.
[45] X. Zhang, Z. Ai, F. Jia, L. Zhang, Generalized one-pot synthesis, characterization, and photocatalytic activity of hierarchical BiOX (X = Cl, Br, I) nanoplate microspheres, J. Phys. Chem. C 112 (2008) 747–753.
[46] J. Olchowka, H. Kabbour, M. Colmont, M. Adlung, C. Wickleder, O. Mentré, $ABiO_2X$ (A = Cd, Ca, Sr, Ba, Pb; X = halogen) Sillen X1 series: polymorphism versus optical properties, Inorg. Chem. 55 (2016) 7582–7592.
[47] D.O. Charkin, P.S. Berdonosov, V.A. Dolgikh, P. Lightfoot, A reinvestigation of quaternary layered bismuth oxyhalides of the Sillén X1 type, J. Solid State Chem. 175 (2003) 316–321.
[48] H. Huang, A.H. Reshak, S. Auluck, S. Jin, N. Tian, Y. Guo, Y. Zhang, Visible-light-responsive Sillén-structured mixed-cationic $CdBiO_2Br$ nanosheets: layer structure design promoting charge separation and oxygen activation reactions, J. Phys. Chem. C 122 (2018) 2661–2672.
[49] Z. Wei, G. Jiang, L. Shen, X. Li, X. Wang, W. Chen, Preparation of Mn-doped BiOBr microspheres for efficient visible-light-induced photocatalysis, MRS Commun. 3 (2013) 145–149.
[50] C. Huang, J. Hua, S. Cong, Z. Zhao, X. Qiu, Hierarchical BiOCl microflowers with improved visible-light-driven photocatalytic activity by Fe(III) modification, Appl. Catal. B 174-175 (2015) 105–112.
[51] C.-Y. Wang, Y.-J. Zhang, W.-K. Wang, D.-N. Pei, G.-X. Huang, J.-J. Chen, X. Zhang, H.-Q. Yu, Enhanced photocatalytic degradation of bisphenol A by Co-doped BiOCl nanosheets under visible light irradiation, Appl. Catal. B 221 (2018) 320–328.
[52] J. Di, J. Xia, S. Yin, H. Xu, L. Xu, Y. Xu, M. He, H. Li, One-pot solvothermal synthesis

of Cu-modified BiOCl via a Cu-containing ionic liquid and its visible-light photocatalytic properties, RSC Adv. 4 (2014) 14281–14290.
[53] M.A. Moyet, R.B. Arthur, E.E. Lueders, W.P. Breeding, H.H. Patterson, The role of copper (II) ions in Cu-BiOCl for use in the photocatalytic degradation of atrazine, J. Environ. Chem. Eng. 6 (2018) 5595–5601.
[54] R.B. Arthur, J.C. Ahern, H.H. Patterson, Application of BiOX photocatalysts in remediation of persistent organic pollutants, Catalysts 8 (604) (2018) 1–25.
[55] J. Lindley, Tetrahedron report number 163: copper assisted nucleophilic substitution of aryl halogen, Tetrahedron 40 (1984) 1433–1456.
[56] D.S. Surry, S.L. Buchwald, Diamine ligands in copper-catalyzed reactions, Chem. Sci. 1 (2010) 13–31.
[57] M. Fan, W. Zhou, Y. Jiang, D. Ma, Assembly of primary (hetero) arylamines via CuI/oxalic diamide-catalyzed coupling of aryl chlorides and ammonia, Org. Lett. 17 (2015) 5934–5937.
[58] W. Zhou, M. Fan, J. Yin, Y. Jiang, D. Ma, CuI/oxalic diamide catalyzed coupling reaction of (hetero)aryl chlorides and amines, J. Am. Chem. Soc. 137 (2015) 11942–11945.
[59] J. Gao, S. Bhunia, K. Wang, L. Gan, S. Xia, D. Ma, Discovery of *N*-(naphthalen-1-yl)-*N'*-alkyl oxalamide ligands enables Cu-catalyzed aryl amination with high turnovers, Org. Lett. 19 (2017) 2809–2812.
[60] G. Chakraborti, S. Paladhi, T. Mandal, J. Dash, "On water" promoted Ullmann-type C-N bond-forming reactions: application to carbazole alkaloids by selective N-arylation of aminophenols, J. Org. Chem. 83 (2018) 7347–7359.
[61] H. Lin, D. Sun, Recent synthetic developments and applications of the Ullmann reaction. A review, Org. Prep. Proced. Int. 45 (2013) 341–394.
[62] M.J. Ajitha, F. Pary, T.L. Nelson, D.G. Musaev, Unveiling the role of base and additive in the Ullmann-type of arene-aryl C–C coupling reaction, ACS Catal. 8 (2018) 4829–4837.
[63] X. Tang, W. Wu, W. Zeng, H. Jiang, Copper-catalyzed oxidative carbon–carbon and/or carbon–heteroatom bond formation with O_2 or internal oxidants, Acc. Chem. Res. 51 (2018) 1092–1105.
[64] P. Zhang, J. Yuan, H. Li, X. Liu, X. Xu, M. Antonietti, Y. Wang, Mesoporous nitrogen-doped carbon for copper-mediated Ullmann-type C–O/–N/–S cross-coupling reactions, RSC Adv. 3 (2013) 1890–1895.
[65] C. Sambiagio, S.P. Marsden, A.J. Blacker, P.C. McGowan, Copper catalysed Ullmann type chemistry: from mechanistic aspects to modern development, Chem. Soc. Rev. 43 (2014) 3525–3550.
[66] F. Monnier, M. Taillefer, Catalytic C–C, C–N, and C–O Ullmann-type coupling reactions, Angew. Chem. Int. Ed. 48 (2009) 6954–6971.
[67] T. Garnier, M. Danel, V. Magné, A. Pujol, V. Bénéteau, P. Pale, S. Chassaing, Copper (I)–USY as a ligand-free and recyclable catalyst for ullmann-type O-, N-, S-, and C-arylation reactions: scope and application to total synthesis, J. Org. Chem. 83 (2018) 6408–6422.
[68] H. Huang, X. Han, X. Li, S. Wang, P.K. Chu, Y. Zhang, Fabrication of multiple heterojunctions with tunable visible-light-active photocatalytic reactivity in BiOBr–BiOI full-range composites based on microstructure modulation and band structures, ACS Appl. Mater. Interfaces 7 (2015) 482–492.
[69] H.W. Huang, K. Xiao, Y. He, T.R. Zhang, F. Dong, X. Du, Y.H. Zhang, In situ assembly of BiOI@$Bi_{12}O_{17}Cl_2$ p-n junction: charge induced unique front-lateral surfaces coupling heterostructure with high exposure of BiOI {001} active facets for robust and nonselective photocatalysis, Appl. Catal. B 199 (2016) 75–86.
[70] Z. Yang, Q. Wang, S. Wei, The synergistic effects of the Cu–CeO_2 (111) catalysts on the adsorption and dissociation of water molecules, Phys. Chem. Chem. Phys. 13 (2011) 9363–9373.
[71] G. Zhao, Y. Tian, H. Fan, J. Zhang, L. Hu, Properties and structures of Bi_2O_3–B_2O_3–TeO_2 glass, J. Mater. Sci. Technol. 29 (2013) 209–214.
[72] M.N. Novokreshchenova, Y. Yukhin, B.B. Bokhonov, Highly pure bismuth (III) oxochloride synthesis, Chem. Sustain. Develop. 13 (2005) 563–568.
[73] P. Balasubramanian, M. Annalakshmi, S.M. Chen, T. Sathesh, T.K. Peng, T.S.T. Balamurugan, Facile solvothermal preparation of Mn_2CuO_4 microspheres: excellent electrocatalyst for real-time detection of H_2O_2 released from live cells, ACS Appl. Mater. Interfaces 10 (2018) 43543–43551.
[74] J.E.D. Davies, Solid state vibrational spectroscopy—III [1] the infrared and Raman spectra of the bismuth (III) oxide halides, J. Inorg. Nucl. Chem. 35 (1973) 1531–1534.
[75] B. Long, Y. Huang, H. Li, F. Zhao, Z. Rui, Z. Liu, X. Tong, H. Ji, Carbon dots sensitized BiOI with dominant {001} facets for superior photocatalytic performance, Ind. Eng. Chem. Res. 54 (2015) 12788–12794.
[76] F. Dong, Y. Sun, M. Fu, Z. Wu, S.C. Lee, Room temperature synthesis and highly enhanced visible light photocatalytic activity of porous BiOI/BiOCl composites nanoplates microflowers, J. Hazard. Mater. 219 (2012) 26–34.
[77] S. Yuvaraj, K. Karthikeyan, D. Kalpana, Y.S. Lee, R.K. Selvan, Surfactant-free hydrothermal synthesis of hierarchically structured spherical $CuBi_2O_4$ as negative electrodes for Li-ion hybrid capacitors, J. Colloid Interface Sci. 469 (2016) 47–56.
[78] Y.F. Zhu, Y.L. Zhu, G.Q. Ding, S.H. Zhu, H.Y. Zheng, Y.W. Li, Highly selective synthesis of ethylene glycol and ethanol via hydrogenation of dimethyl oxalate on Cu catalysts: influence of support, Appl. Catal. A Gen. 468 (2013) 296–304.
[79] X. Zhang, L. Zhang, T. Xie, D. Wang, Low-temperature synthesis and high visible-light-induced photocatalytic activity of BiOI/TiO_2 heterostructures, J. Phys. Chem. C 113 (2009) 7371–7378.
[80] M. Sun, J. Hu, C. Zhai, M. Zhu, J. Pan, A pn heterojunction of CuI/TiO_2 with enhanced photoelectrocatalytic activity for methanol electro-oxidation, Electrochim. Acta 245 (2017) 863–871.
[81] J. Yu, J. Ran, Facile preparation and enhanced photocatalytic H_2-production activity of $Cu(OH)_2$ cluster modified TiO_2, Energy Environ. Sci. 4 (2011) 1364–1371.
[82] H. Xu, J. Yan, Y. Xu, Y. Song, H. Li, J. Xia, C. Huang, H. Wan, Novel visible-light-driven AgX/graphite-like C_3N_4 (X= Br, I) hybrid materials with synergistic photocatalytic activity, Appl. Catal. B 129 (2013) 182–193.
[83] T. Umebayashi, K. Asai, T. Kondo, A. Nakao, Electronic structures of lead iodide based low-dimensional crystals, Phys. Rev. B 67 (155405) (2003) 1–6.
[84] W.E. Morgan, J.R. van Wazer, W.J. Stec, Inner-orbital photoelectron spectroscopy of the alkali metal halides, perchlorates, phosphates, and pyrophosphates, J. Am. Chem. Soc. 95 (1973) 751–755.
[85] H. Lin, H. Ye, X. Li, J. Cao, S. Chen, Facile anion-exchange synthesis of BiOI/BiOBr composite with enhanced photoelectrochemical and photocatalytic properties, Ceram. Int. 40 (2014) 9743–9750.
[86] V. Subbaramaiah, V.C. Srivastava, I.D. Mall, Optimization of reaction parameters and kinetic modeling of catalytic wet peroxidation of picoline by Cu/SBA-15, Ind. Eng. Chem. Res. 52 (2013) 9021–9029.
[87] M. Long, P. Hu, H. Wu, Y. Chen, B. Tan, W. Cai, Understanding the composition and electronic structure dependent photocatalytic performance of bismuth oxyiodides, J. Mater. Chem. A 3 (2015) 5592–5598.
[88] H. Huang, K. Xiao, T. Zhang, F. Dong, Y. Zhang, Rational design on 3D hierarchical bismuth oxyiodides via in situ self-template phase transformation and phase-junction construction for optimizing photocatalysis against diverse contaminants, Appl. Catal. B 203 (2017) 879–888.
[89] X. Xiao, Y. Lin, B. Pan, W. Fan, Y. Huang, Photocatalytic degradation of methyl orange by BiOI/$Bi_4O_5I_2$ microspheres under visible light irradiation, Inorg. Chem. Commun. 93 (2018) 65–68.
[90] Y. Wang, C. Liu, Y. Zhang, W. Meng, B. Yu, S. Pu, D. Yuan, F. Qi, B. Xu, W. Chu, Sulfate radical-based photo-Fenton reaction derived by $CuBi_2O_4$ and its composites with α-Bi_2O_3 under visible light irradiation: catalyst fabrication, performance and reaction mechanism, Appl. Catal. B 235 (2018) 264–273.
[91] T.B. Li, G. Chen, C. Zhou, Z.Y. Shen, R.C. Jin, J.X. Sun, New photocatalyst BiOCl/BiOI composites with highly enhanced visible light photocatalytic performances, Dalton Trans. 40 (2011) 6751–6758.
[92] M. Fan, W. Zhou, Y. Jiang, D. Ma, Assembly of primary (hetero) arylamines via CuI/oxalic diamide-catalyzed coupling of aryl chlorides and ammonia, Org. Lett. 17 (2015) 5934–5937.
[93] S.L. Scott, A matter of life(time) and death, ACS Catal. 8 (2018) 8597–8599.